Available online at www.sciencedirect.com
SCIENCE DIRECT®
Journal of Catalysis 225 (2004) 128–137
JOURNAL OF CATALYSIS
www.elsevier.com/locate/jcat

Catalytic oxidation of pyridine on the supported copper catalysts in the presence of excess oxygen

J. Zhou, Q.-H. Xia,* S.-C. Shen, S. Kawi, and K. Hidajat

Department of Chemical and Environmental Engineering, National University of Singapore, Singapore, Republic of Singapore

Received 19 September 2003; revised 24 March 2004; accepted 24 March 2004

Available online 12 May 2004

Abstract

The catalytic oxidation of pyridine pollutant on a series of supported metals/zeolites catalysts in the presence of excess oxygen was studied. All the catalysts were further characterized by means of BET, XRD, H_2-TPR, XPS, and FTIR techniques. The catalyst that could be reduced at lower temperatures had a better oxidation activity. The better NO_x control ability could be attributed to the importance of the Lewis acidity of the samples, rather than to that of Brønsted acidity. On supported copper catalysts, $Cu(H_2O)_6^{2+}$ ions had higher activity for the NO_x control but poorer activity for the pyridine oxidation. The cointeraction of some factors, such as the surface acidity of catalysts, the structure of supports, and the amount of $Cu(H_2O)_6^{2+}$ ions on the supports, played a deciding role in the NO_x control ability of the catalysts. Comparatively, Cu/beta was the most active for the pyridine oxidation and NO_x control, possibly being a potential catalyst for the catalytic removal of pyridine pollutant.

Keywords: Supported copper catalysts; Cu/β; Catalytic oxidation of pyridine; NO_x yield

1. Introduction

Nowadays vehicle exhaust as a major source of air pollution is attracting increasing attention from governments and society. Nitrated polycyclic aromatic hydrocarbons (NPAC) have been identified as potent mutagens and possible carcinogens. Since 1977, when the EPA (Environment Protection Association of America) first identified diesel exhaust particulates as mutagens, NPAC has been thought to be responsible for up to 90% of the total mutagenicity of diesel particulates. Although much research has been performed to determine the concentration of NPAC in the diesel exhaust, the reports on the removal of NPAC from the diesel exhaust are quite limited. Since the automobile emission legislation is becoming stringent, the automotive industry is interested in the development of a catalyst applied for removing NPAC from the exhaust of diesel engines. For understanding the catalytic decomposition of nitro-PACs, nitro-compounds may be more suitable than pyridine as the model compounds. Indeed, Ismagilov et al. [1] reported higher NO_x yield from nitrobenzene than from pyridine when both were catalytically oxidized. However, as one important pollutant, the catalytic oxidation of pyridine has been extensively investigated, which thus led to our studies on the oxidation decomposition of pyridine over a series of zeolite-supported catalysts.

To date, there have been two main routes dealing with the catalytic removal of pyridine. One is the catalytic oxidation (or the catalytic combustion), the other is the catalytic supercritical water oxidation (CSCWO). The catalytic oxidation of pyridine was reported in 1983 by Ismagilov et al. [2,3], who observed the formation of nitrogen oxides in the catalytic oxidation of pyridine over the catalysts, such as 0.64% Pt/γ-Al_2O_3, 26% CuO/γ-Al_2O_3, 5% $CuCr_2O_4$/γ-Al_2O_3, 11% CuO/γ-Al_2O_3, and 30% $CuCr_2O_4$/γ-Al_2O_3. All the catalysts showed similar specific activity toward the oxidation of pyridine, and the oxides catalyst exhibited much better NO_x control ability (the ability to control the yield of NO_x) than the platinum one. It was found that the NO_x control ability tended to decrease in the order of 30% $CuCr_2O_4$/γ-Al_2O_3 > 11% CuO/γ-Al_2O_3 > 5% $CuCr_2O_4$/γ-Al_2O_3. They also reported that at temperatures between 240 and 550 °C, the main products were CO_2, H_2O,

* Corresponding author.
E-mail address: xia1965@yahoo.com (Q.-H. Xia).

0021-9517/$ – see front matter
doi:10.1016/j.jcat.2004.03.042

N_2, and NO_x, in which the yield of NO_x increased with the increase of temperature.

Luo et al. [4] studied the pyridine oxidation over γ-Al_2O_3-supported metal oxide catalysts, such as Ag/γ-Al_2O_3, Cu/γ-Al_2O_3, Mn/γ-Al_2O_3, Cr/γ-Al_2O_3, Fe/γ-Al_2O_3, Co/γ-Al_2O_3, Ni/γ-Al_2O_3, V/γ-Al_2O_3, and Ce/γ-Al_2O_3. They found that the content of NO_x generating from the pyridine combustion went through a maximum value as the temperature increased, and that the oxidation activity of individual catalyst was proportional to its NO_x control ability. The oxidation activity and NO_x control ability of the catalysts decreased in the sequence Ag/γ-Al_2O_3 > Cu/γ-Al_2O_3 > Mn/γ-Al_2O_3 > Cr/γ-Al_2O_3 > Fe/γ-Al_2O_3 ≈ Co/γ-Al_2O_3 > Ni/γ-Al_2O_3, V/γ-Al_2O_3 > Ce/γ-Al_2O_3. The results further showed that the oxidation activity and NO_x control ability of individual Ag/γ-Al_2O_3 catalyst could be promoted by certain amount of Mn or Co. Their other researches showed that increasing the metal loading remarkably improved the oxidation activity and NO_x control ability of the catalyst until reaching an equilibrium value [5]. They further suggested that the ability of the catalyst to control the formation of NO_x species be closely relevant to the acidity on the catalyst surface.

Crain et al. [6] reported the catalytic supercritical water oxidation of pyridine in the temperature range of 425–527 °C, in which the conversion of pyridine increased from 0.03 (at 426 °C) to 0.68 (a.u.) (at 527 °C) at a residence time of 10 s. During the CSCWO of pyridine, ammonia, dimethylamine, and several carboxylic acids such as formic acid, acetic acid, glutaconic acid, and oxalic acid could be detected. Wightman et al. [7] reported the CSCWO of pyridine in a flowing system with a conversion of around 16% (at 400 °C and a pressure of 40.82 MPa). Katritzky and Barcock [8] observed that pyridine was nonreactive in the absence of oxygen, even in supercritical water. Aki and Abraham [9] reported the absence of external mass-transfer limit and the presence of internal mass-transfer limit during the CSCWO of pyridine over Pt/γ-Al_2O_3.

As noted above, research on the catalytic removal of pyridine has been carried out over metal oxide-supported catalysts such as Pt/γ-Al_2O_3 or CuO/γ-Al_2O_3. However, no study has been, to date, focused on the zeolite-supported catalysts, which are being widely used in the SCR-deNO_x reaction and petrochemical industry. The aim of this work is to test the catalytic oxidation of pyridine over zeolite-supported catalysts and to compare the difference in their activities for the oxidation of pyridine.

2. Experimental

2.1. Preparation of catalysts

Supported-copper catalysts were prepared by wet impregnation of powder support solids with an aqueous copper(II) nitrate solution. Excess water was evaporated off at 90 °C under stirring. The samples were, then, dried at 100 °C for 12 h, followed by fine grinding, and calcination at 700 °C for 10 h in the dry air. Metal/beta catalysts were also prepared by wet impregnation of zeolite β with the aqueous solutions containing different metal salts, such as cobalt acetate, nickel nitrate, and iron sulfate. The powdered support materials used were beta, ZSM-5, MCM-41, and γ-Al_2O_3 (Strem Chemicals, USA). Zeolite beta with a Si/Al ratio of 20 was synthesized according to the procedure reported elsewhere [10]. Zeolite ZSM-5 with a Si/Al ratio of 15 was synthesized hydrothermally at 170 °C using tetrapropylammonium hydroxide (TPAOH) as the structure-directing agent [11,12]. The mesoporous MCM-41 with a Si/Al ratio of 20 was hydrothermally synthesized at 100 °C using C_{16}TMABr as a template [13,14]. The removal of organic template molecules was carried out by calcinations at 550 °C for 10 h in a flowing air. Note that the unit of metal loadings on the support was wt%.

2.2. Characterization of catalysts

Autosorb-1 was used to determine the N_2 adsorption–desorption isotherms of the samples. The BET specific surface area was calculated in terms of the Brunauer–Emmett–Teller (BET) equation. The BJH method was used to calculate the pore volume and the pore-size distributions of the samples. Prior to the measurements, the samples were degassed at 300 °C under a vacuum of 10^{-2} mbar for 10 h.

X-ray diffraction (XRD) analysis was carried out using a Shimadzu XRD-6000 diffractometer with Ni-filtered Cu-K_α radiation operating at 40 kV and 30 mA. The scanning conditions for ZSM-5, beta, and Al_2O_3 were as follows: divergence slit, 1.0 (°); scattering slit, 1.0 (°); and receiving slit, 0.3 (mm). The scanning range was from 5 to 80° 2θ with a scanning speed of 2°/min. The measuring conditions for MCM-41 were changed to divergence slit, 0.05 (°); scattering slit, 1.0 (°); and receiving slit, 0.15 (mm), with a scanning range from 1.5 to 10° 2θ. Temperature-programmed reduction (TPR) was carried out in a He flow of 50 ml/min (5 vol% H_2), from room temperature to 800 °C at a heating rate of 5 °C/min. A TCD was used to monitor the H_2 consumption. Before starting the TPR procedure, the sample was pretreated at 500 °C for 1 h in a helium flow of 100 ml/min and then cooled down to room temperature.

X-ray photoelectron spectroscopy (XPS) spectra were recorded on a Shimadzu Kratos AXIS spectrometer, using a monochromatic Al-K_α radiation (1486.6 eV, 225 W), operating at a constant transmission energy pass (80 eV). The C 1s photoelectron peak (binding energy at 284.6 eV with an accuracy of ±0.2 eV) was used as an energy reference. All the spectra were fitted using a Gaussian method in order to determine the number of components in the peaks. Shirley background was subtracted in the least-square fitting. The peak shape was fixed to a mixture of 20% Lorentzian and 80% Gaussian with an asymmetric parameter of 0.

IR spectra of adsorbed pyridine were recorded to determine the presence of Brønsted and Lewis acid sites over

the catalysts, which was performed using a Shimadzu FTIR-8700 spectrophotometer with a resolution of 2 cm^{-1} and connected to a PFEIFFER vacuum system. Fifteen milligrams of the sample was ground and then pressed into a self-supporting wafer at the pressure of 6000 kg/cm^2 for 15 min, which was then mounted into a quartz IR cell with CaF_2 windows. Before scanning, the self-supporting wafer of the catalyst was heated at 400 °C for 3 h under a residual pressure of 10^{-6} mbar before adsorbing an excess of pyridine at room temperature, followed by evacuation at 200 °C for 30 min. Note that the FTIR background was in situ recorded at room temperature at a vacuum of 10^{-6} mbar without adsorbing pyridine after the self-supporting wafer had been pretreated at 400 °C for 3 h under a residual pressure of 10^{-6} mbar. Brønsted and Lewis were quantified from the integrated areas of the bands at 1540 and at 1445 cm^{-1}, respectively. The integrated areas of these two bands provide information only about the relative amount of pyridine, which interacts with Brønsted and Lewis sites; therefore the B and L values must be regarded as relative indications.

2.3. Catalytic tests

The reaction was carried out in a fixed-bed microreactor, loaded with 0.3 g of the catalyst, operating at normal pressure in the temperature range 250–700 °C with a feed gas (120 ml/min) consisting of 600 ppm pyridine and 5% O_2 in helium. Each reaction reached steady state in 30 min; the products were then analyzed on stream by a Shimadzu GC-17A gas chromatograph in order to detect the composition under steady state. The conversion of pyridine and the yield of NO_x were, respectively, calculated based on the inlet and outlet compositions of the reactor, namely, $X_{pyr} =$ (inlet pyridine − outlet pyridine)/(inlet pyridine) × 100% and the yield of NO_x = (the detected concentration of NO_x)/(the theoretical concentration of NO_x) × 100%. An on-line Shimadzu NOA-7000 NO_x analyzer monitored the concentration of NO_x in the effluent gas. A parameter T_{100}, characterizing the pyridine oxidation ability of the catalysts, was defined as the lowest temperature at which 100% of pyridine conversion was realized. Generally, the lower the T_{100} value, the higher the pyridine oxidation ability of the catalyst. $T_{NO_x,5\%}$ stood for the temperature at which the yield of NO_x is 5%. Note that a new parameter ΔT was defined as $(T_{NO_x,5\%} - T_{100})$, where the bigger the ΔT value, the better the NO_x control ability the catalyst retained.

3. Results and discussion

3.1. Effect of copper content on the activity of catalysts

Copper, which is a cheap metal compared with cobalt and nickel, as an active metal component has been widely applied in the SCR deNO_x reaction, to achieve a rather high deNO_x activity. It is well known that the loading amount of active component has a great impact on the performance of the catalyst [2,3], and highly dispersed active particles have higher activity than big crystal particles. Many studies have shown that the activity of catalysts cannot be infinitely improved through simply increasing the content of active component when it has reached a certain value, in which the relationship between the activity and the loading shows a bell-shaped curve. In this research, copper/beta zeolite sample was used as the catalyst. To investigate the effect of copper loading on the pyridine oxidation activity and the NO_x control ability of Cu/beta catalysts, the copper loading was varied from 0 to 15% (wt%).

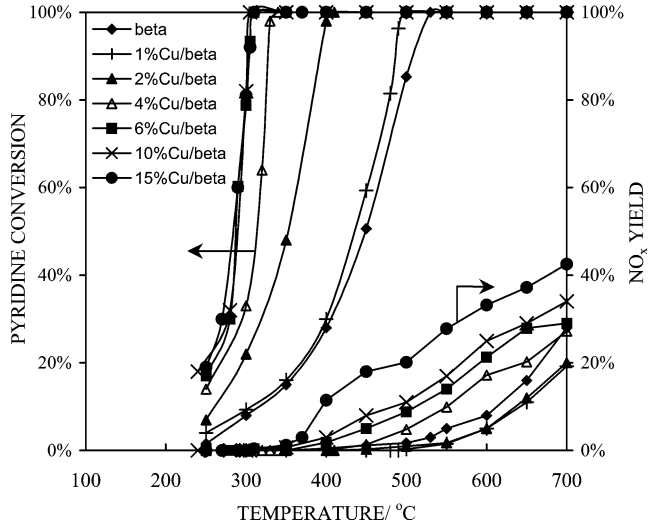

Fig. 1. Effect of copper loading on the pyridine conversion and NO_x control.

Table 1
Characteristic temperatures and BET surface areas of Cu/beta catalysts with different copper loadings

Catalysts	T_{100} (°C)	$T_{NO_x,5\%}$ (°C)	ΔT (°C)	BET specific surface area (m^2/g)
Beta	530	550	20	542
1% Cu/beta	500	600	100	516
2% Cu/beta	410	600	190	500
4% Cu/beta	340	500	160	464
6% Cu/beta	310	450	140	398
10% Cu/beta	305	420	115	381
15% Cu/beta	310	395	85	368

T_{100}: the lowest temperature at which the pyridine conversion is 100%.
$T_{NO_x,5\%}$: the temperature at which the yield of NO_x is 5%.
$\Delta T = T_{NO_x,5\%} - T_{100}$: an indication of the NO_x control ability.

Fig. 1 and Table 1 show the pyridine conversion and NO_x yield as a function of temperature over the catalysts, where the curves on the left correspond to the pyridine conversion, while ones on the right correspond to the NO_x yield. The activity of 1% Cu/beta for the pyridine oxidation was slightly better than that of pure beta. A parameter T_{100}, characterizing the ability of the catalysts to oxidize pyridine, was defined as the lowest temperature at which 100% of pyridine conversion was realized. Generally, the lower the T_{100} value, the higher the ability of the catalyst to oxidize pyri-

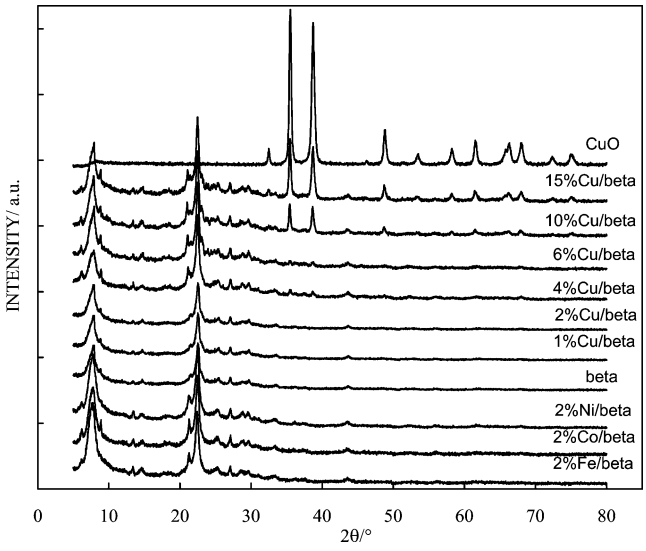

Fig. 2. XRD patterns of Cu/beta with different copper loadings and different metals/beta samples.

dine. The T_{100} values of 1% Cu/beta and pure beta were 500 and 530 °C, respectively. When the copper content was increased to 2 wt%, the oxidation activity of the catalyst was much improved, with an obvious decrease of T_{100} value to 410 °C. With a continuous increase of the copper content to 4 wt%, the oxidation activity of the resulting catalyst was further improved, accompanied with an abrupt reduction of T_{100} value to 340 °C. However, when the copper content was increased to 6 wt%, the improvement of oxidation activity of the resultant catalyst was badly limited, with a quite small drop of T_{100} value to 310 °C. Whereas, the copper loadings of 10 and 15 wt% showed a similar activity for the pyridine oxidation to that of 6 wt%, where T_{100} values of three catalysts were 310 (6 wt% Cu), 305 (10 wt% Cu), 310 °C (15 wt% Cu), respectively, with an almost same pyridine conversion behavior, in agreement with the phenomenon of pyridine oxidation over Ag/γ-Al_2O_3 catalysts with different silver loadings reported by Luo et al. [4]. Based on the variation of T_{100} value, the oxidation activity of all the copper/beta catalysts increased in the following sequence: beta ($T_{100} = 530$ °C) < 1% Cu/beta (500 °C) < 2% Cu/beta (410 °C) < 4% Cu/beta (340 °C) < 6% Cu/beta (310 °C) ≈ 10% Cu/beta (305 °C) ≈ 15% Cu/beta (310 °C).

The XRD patterns (in Fig. 2) of the catalysts show that below 6 wt% of the copper content on zeolite beta, only zeolite beta diffraction peaks are observed. Neither CuO nor metal Cu diffraction peaks were detected under our experimental conditions, indicating that all the copper on beta has been highly dispersed with smaller than 5 nm of the particle size. However, it is not the case for 10% Cu/beta and 15% Cu/beta catalysts, which present rather clear diffraction peaks of crystalline CuO oxides in their XRD patterns, indicative of the formation of big CuO crystals on zeolite beta. Moreover, increasing the copper loading from 10 to 15 wt% further promoted the growth of big CuO crystal particles.

Both 1% Cu/beta and 2% Cu/beta catalysts exhibited a similar NO_x yield curve (in Fig. 1). For other four catalysts 4% Cu/beta, 6% Cu/beta, 10% Cu/beta, and 15% Cu/beta, despite their similar pyridine oxidation activities, their NO_x yield behaviors were noticeably different from one another. For example, at 500 °C the NO_x yield of 4% Cu/beta was 4.8%, and that of 15% Cu/beta was 20.1%. When the temperature was increased to 700 °C, the NO_x yield of 4% Cu/beta increased to 27.2%, while that of 15% Cu/beta even to 42.5%. Table 1 presents the characteristic temperatures of the catalysts, which are used to evaluate the activity of the catalysts. From Table 1, we can observe that the NO_x control ability ($\Delta T = T_{NO_x,5\%} - T_{100}$) of the catalysts first shows an increase trend with increasing the copper content from 0 to 2 wt%, then decreases with a further increase of copper content to above 2 wt%, typical of a clear bell-shaped curve. Amongst the Cu/beta catalysts, 2% Cu/beta retained the best NO_x control ability. BET data in Table 1 clearly show that increasing the copper content in the range of 1–6 wt% largely retarded the specific surface area of the catalysts, which is in agreement with those for the catalysts used in the carbon monoxide and methane oxidation [15], but strikingly improved the pyridine oxidation activity of the catalyst. However, when the copper loading was above 6 wt%, the pyridine conversion (T_{100} value) could not be correlated with the specific surface area at all.

3.2. Effect of different metals on the activity of catalysts

3.2.1. Property and oxidation activity of catalysts

In this study, zeolite beta-supported copper (Cu), cobalt (Co), iron (Fe), and nickel (Ni) catalysts were tested. Since 2% Cu/beta showed the best NO_x control ability (which is the most concerned, more than the pyridine oxidation ability), the metal loading in the unspecified studies is maintained at about 2 wt%. The BET surface area and total pore volume of the resulting catalysts are shown in Table 2. The surface areas of all the catalysts were in the range of 471–500 m^2/g, without significant decrease of the BET surface area for all the samples. On the other hand, the total pore volumes of the catalysts kept more or less constant ranging from 0.30 to 0.32 cm^3/g. The results suggest that partial blockage of some pores has occurred due to the metal-species dispersion either in the channels or outer surface of beta zeolite. As shown in Fig. 2, only diffraction peaks of beta are detected for four catalysts without any diffraction peaks of metal oxides, indicative of the high dispersion of these metal oxide constituents on the surface of beta.

For the catalytic oxidation of pyridine, the ideally expected reaction is to combust pyridine completely into CO_2, H_2O, N_2, and NO_x. The lesser amount of NO_x the catalyst produces, the better its performance. Fig. 3 depicts the relation of pyridine conversion and NO_x yield to temperature over beta-supported metal catalysts. Pyridine conversion and NO_x yield increase with increasing the reaction temperature, consistent with those observed by Ismagilov et al. [2,3] but

Table 2
Specific surface area and total pore volume of beta supported metal catalysts

Catalysts	BET surface area (m^2/g)	Total pore volume (cm^3/g)
Beta	542	0.33
2% Cu/beta	500	0.32
2% Co/beta	472	0.30
2% Ni/beta	491	0.31
2% Fe/beta	473	0.30

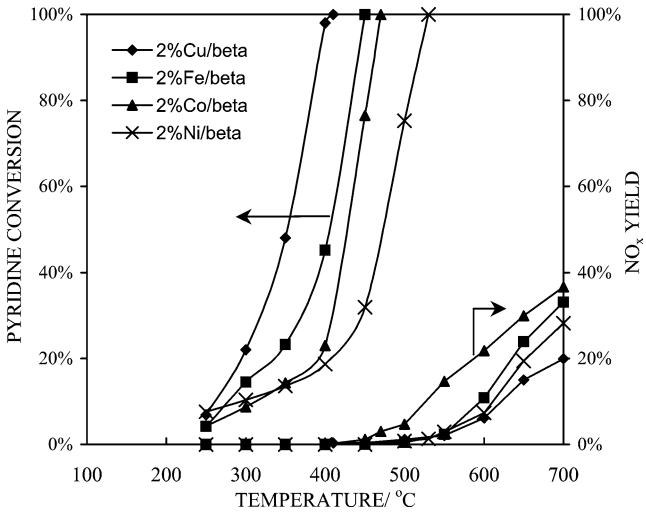

Fig. 3. Pyridine conversion and NO_x yield over different beta-supported metal catalysts.

different from the results of Luo et al. [4], who found that the NO_x yield went through a maximum value as the temperature increased. The difference may result from different reactant compositions, in which the reactant mixture used by Luo was 500 ppm pyridine in air, while ours was 600 ppm in helium balanced with 5% O_2. Table 3 lists the characteristic temperatures of pyridine oxidation over various catalysts, at which temperature 100% conversion of pyridine was realized. Comparatively, 2% Cu/beta still exhibited the best pyridine oxidation activity and NO_x control ability, and its T_{100} and ΔT values were 410 and 190 °C, respectively. The oxidation activity of these catalysts decreased in the order of 2% Cu/beta > 2% Fe/beta > 2% Co/beta > 2% Ni/beta; while their NO_x control ability showed a new sequence 2% Cu/beta > 2% Fe/beta > 2% Co/beta ≈ 2% Ni/beta. The results show that the catalyst with a better pyridine oxidation activity also retains a stronger NO_x control ability, in agreement with that of Luo et al. [4].

3.2.2. *Temperature-programmed reduction tests*

TPR tests were conducted to determine the chemical state of metals on zeolite beta. In the TPR profiles of four beta-supported metal catalysts, two main peaks at 222 and 332 °C with a shoulder at 262 °C were observed for the sample 2% Cu/beta (in Fig. 4). According to the reports [16–18], the reactions involved in the copper-containing catalysts proceed

Table 3
Characteristic temperatures of pyridine oxidation on various catalysts

Catalysts	T_{100} (°C)	$T_{NO_x,5\%}$ (°C)	ΔT (°C)
2% Cu/beta	410	600	190
2% Fe/beta	450	560	110
2% Co/beta	470	500	30
2% Ni/beta	530	560	30

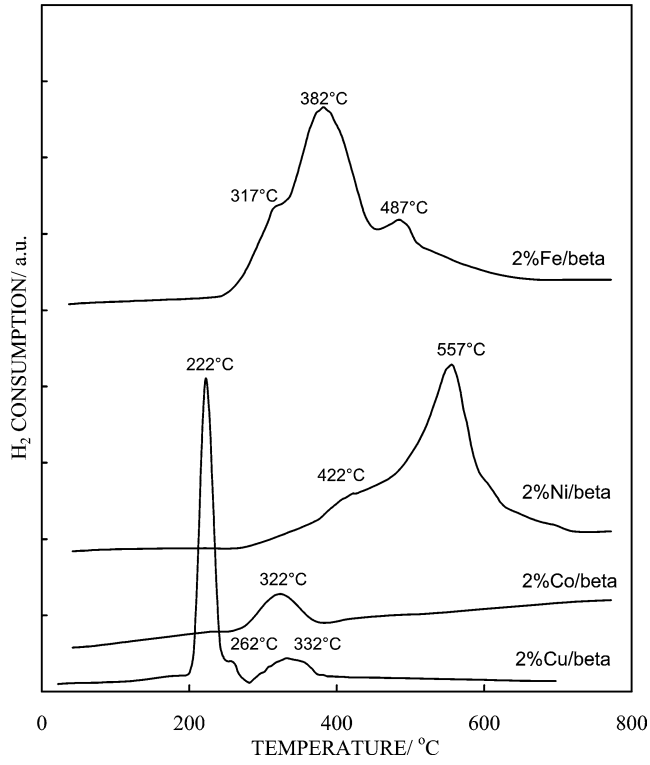

Fig. 4. H_2-TPR profiles of different beta-supported metal catalysts.

in the following mechanism:

$$CuO + H_2 \rightarrow Cu^0 + H_2O, \quad (1)$$

$$Cu^{2+} + 0.5H_2 \rightarrow Cu^+ + H^+, \quad (2)$$

$$Cu^+ + 0.5H_2 \rightarrow Cu^0 + H^+, \quad (3)$$

where reactions (1) and (2) occur at a lower temperature than reaction (3) [19]. Thus, the first peak at 222 °C for the sample 2% Cu/beta is ascribable to the reduction of CuO to metal Cu^0, and the shoulder at 262 °C is assigned to that of Cu^{2+} to Cu^+, while the peak at 332 °C is the signal of reduction of Cu^+ species to metal Cu^0. The TPR profile of the sample 2% Co/beta shows one small peak centering at 322 °C, attributable to the reduction of cobalt oxides deposited outside the zeolite [20]. The absence of reduction peaks from Co^{2+} to Co^+ or to metal Co^0 is not surprising, as Co^{2+} species is not readily reduced to Co^+ or to metal Co^0 [21].

TPR profile of 2% Fe/beta shows that the reduction of iron species occhree steps with a maximum signal at 317, 382, and 487 °C, respectively. According to the literature [22–24], the reduction of unsupported or supported Fe_2O_3

to metal Fe^0 occurs in three steps below 630 °C, with Fe_3O_4 and FeO as the intermediates. The reduction of Fe^{3+} species to metal Fe^0 in the charge compensation sites of zeolite requires the temperatures above 730 °C, but that of Fe^{3+} to Fe^{2+} is observed to occur at lower temperatures [25–27]. Therefore, the former two peaks could be assigned to the reduction of Fe_2O_3 "clusters" to metal Fe^0, with Fe_3O_4 as intermediate species [28,29], and the third one corresponding to the reduction of Fe^{3+} to Fe^{2+} [30,31], where Fe^{3+} species come from the oxidation of ion-exchanged Fe^{2+} ions into zeolite by calcinations [32].

A main peak locating at 557 °C, together with a very small shoulder at 422 °C, is observed in the TPR profile of 2% Ni/beta. According to the literature [33,34], the main peak at 557 °C is ascribable to the reduction of Ni^{2+} locating in 12-ring channels [35], while the shoulder at 422 °C to the reduction of NiO oxide to metal Ni^0. As shown in Fig. 4, the reduction temperature of the samples displays a decreases in the order of 2% Ni/beta > 2% Co/beta > 2% Fe/beta > 2% Cu/beta, inversely proportional to that of pyridine oxidation activity of these catalysts: 2% Cu/beta > 2% Fe/beta > 2% Co/beta > 2% Ni/beta (in Fig. 3), suggesting that the metal reduced readily at a lower temperature has higher oxidation activity.

3.3. Effect of different supports on the activity of catalysts

3.3.1. Structures of different supports

The copper-loaded catalysts on different supports were prepared by wet impregnation. It was reported that the support took an important role in the catalyst activity. In this work, the effect of supports was investigated on the catalysts of Cu/γ-Al_2O_3, Cu/ZSM-5, Cu/beta, and Cu/MCM-41 with a loading of 2 wt% Cu, which is an optimal value for showing the best NO_x control ability of 2% Cu/beta catalyst. The X-ray diffraction patterns of ZSM-5 and beta show that both are highly crystallized. The XRD pattern of MCM-41 displays a sharp peak of d_{100} at 39 Å, without distinct peaks of (110), (200), and (210), suggesting its short-range ordered mesostructure after the aluminum incorporation. The diffraction intensity of γ-Al_2O_3 is not so strong as those of zeolites ZSM-5 and beta.

Table 4 reports the BET surface area and total pore volume of supports and catalysts. The results show that the impregnation of copper on the supports led to a decrease of surface area and total pore volume of the catalysts, indicative of the partial blockage of some pores of these supports by the loaded copper. Compared with pure MCM-41, the surface area and total pore volume of 2% Cu/MCM-41 are reduced a lot.

3.3.2. Contribution of supports to the oxidation activity

To reveal the effect of support materials on the activity of catalysts, the pyridine oxidation was directly conducted over pure supports, such as beta, ZSM-5, MCM-41, and γ-Al_2O_3. Fig. 5 has shown that the NO_x control ability of different supports decreases in the order of beta > ZSM-5 > γ-Al_2O_3 > MCM-41, in agreement with the order of 2% Cu/beta > 2% Cu/ZSM-5 > 2% Cu/γ-Al_2O_3 ≈ 2% Cu/MCM-41 depicted in Fig. 6, where the introduction of copper species noticeably improved both the oxidation activity and the NO_x control ability of the catalysts but did not change the trend of NO_x control ability of the supports. This suggests that the NO_x control ability of supported copper catalysts is, at least partially, determined by the nature of the supports.

Table 4
Specific surface area and total pore volume of different supports and catalysts as well as surface acidity of different supports

Sample	BET surface area (m^2/g)	Total pore volume (cm^3/g)	B acid (1540 cm^{-1})	L acid (1445 cm^{-1})
Beta	542	0.34	1.66	4.23
ZSM-5	256	0.15	3.80	1.05
MCM-41	1330	1.04	0.59	0.62
γ-Al_2O_3	128	0.23	1.41	0.75
2% Cu/beta	500	0.32		
2% Cu/ZSM-5	235	0.15		
2% Cu/MCM-41	695	0.47		
2% Cu/γ-Al_2O_3	94	0.16		

Brønsted and Lewis acidities are quantified into integrated areas of the absorbances at 1540 cm^{-1} and at 1445 cm^{-1}, respectively.

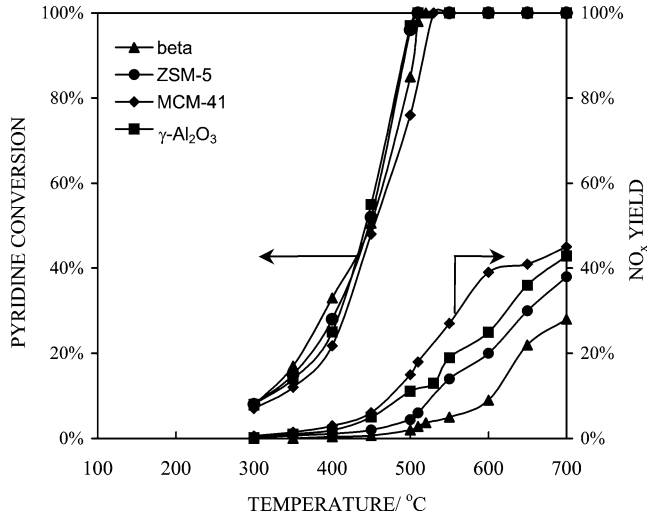

Fig. 5. Pyridine conversion and NO_x yield over different supports.

The surface acidity of the supports was determined by the FTIR spectrum of pyridine adsorption, and Brønsted and Lewis acidities were quantified from the integrated areas of the bands at 1540 and 1445 cm^{-1}, respectively. Fig. 7 shows that beta and ZSM-5 are more acidic than γ-Al_2O_3 and MCM-41, in which the total acidity of γ-Al_2O_3 is stronger than that of MCM-41, corresponding to the tendency of NO_x control ability of the supports. The data in Table 4 show that the number of Brønsted acid sites of four acidic supports decreases in the following sequence, ZSM-5 (3.80) > beta (1.66) > γ-Al_2O_3 (1.41) > MCM-41 (0.59); while that of their Lewis acid sites decrease in a new order

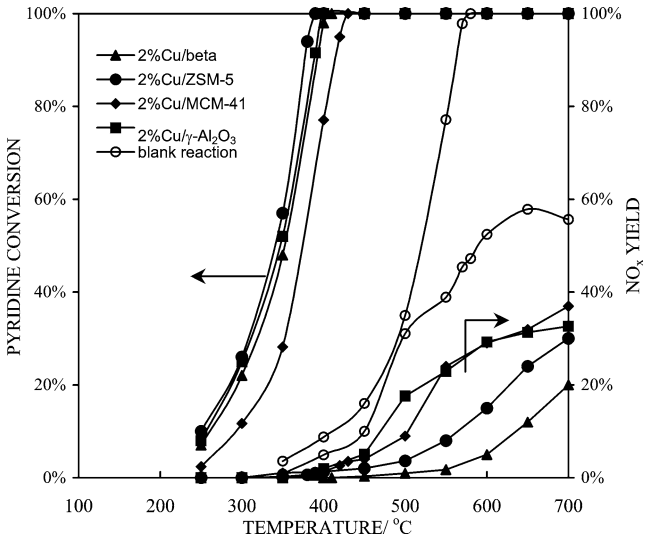

Fig. 6. Pyridine conversion and NO_x yield over different supported copper catalysts.

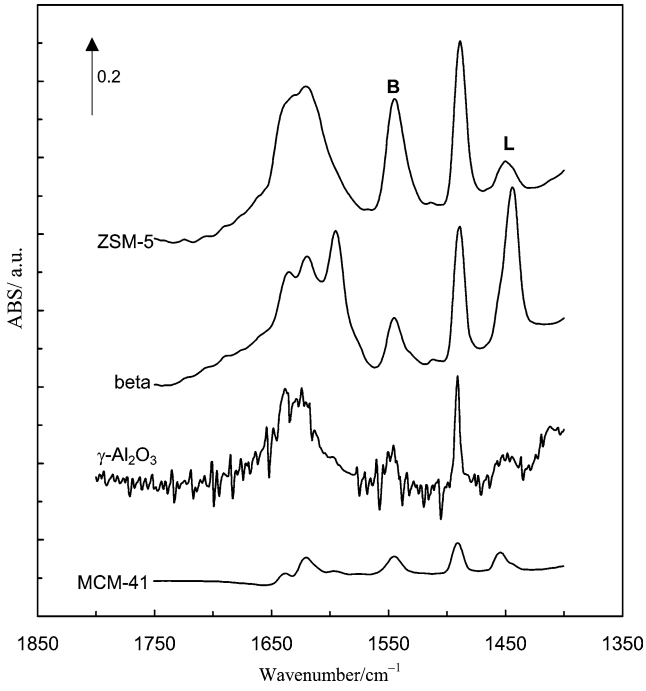

Fig. 7. Pyridine-adsorption FTIR spectra of different supports.

of beta (4.23) > ZSM-5 (1.05) > γ-Al_2O_3 (0.75) > MCM-41 (0.62), consistent with their NO_x control ability order of beta > ZSM-5 > γ-Al_2O_3 > MCM-41. It seems that the better NO_x control ability can be attributed to the importance of Lewis acidity of samples, rather than to that of Brønsted acidity. Especially, beta showed a better NO_x control ability than ZSM-5, but the Brønsted acidity of beta (1.66) was much weaker than that of ZSM-5 (3.80). This phenomenon could be partially assigned with the structure of beta and ZSM-5. It can be assumed that pyridine molecules or NO_x molecules resulting from the pyridine oxidation could readily diffuse into or out of large pores (~ 7 Å) of beta instead of small pores (~ 5.5 Å) of ZSM-5, thus, leading to the better NO_x control ability of zeolite beta [36].

Table 5
Characteristic temperatures of different copper-loaded catalysts

Catalysts	T_{100} (°C)	$T_{NO_x,5\%}$ (°C)	ΔT (°C)
2% Cu/beta	410	600	190
2% Cu/ZSM-5	390	520	130
2% Cu/MCM-41	430	450	20
2% Cu/γ-Al_2O_3	400	450	50

3.3.3. Activity of copper-loaded catalysts

Fig. 6 illustrates the pyridine conversion and NO_x yield over different copper-loaded catalysts. 2% Cu/beta, 2% Cu/ZSM-5, and 2% Cu/γ-Al_2O_3 exhibited a similar pyridine oxidation activity tendency and a close T_{100} value about 390 °C. 2% Cu/MCM-41 was less active for the pyridine oxidation as its T_{100} value was high up to 430 °C. These catalysts have shown quite different NO_x control abilities, which are clearly shown on the right-hand side in Fig. 6. At a reaction temperature as high as 700 °C, the NO_x yield of 2% Cu/beta, 2% Cu/ZSM-5, 2% Cu/MCM-41, and 2% Cu/γ-Al_2O_3 was 20, 30, 37, and 33%, respectively. The oxidation activity of pyridine on these catalysts shows a descending tendency of 2% Cu/ZSM-5 > 2% Cu/γ-Al_2O_3 > 2% Cu/beta > 2% Cu/MCM-41.

The characteristic temperatures of the catalysts are listed in Table 5. The lowest $T_{100} = 390$ °C value showed the best pyridine oxidation activity of 2% Cu/ZSM-5 catalyst; in contrast, 2% Cu/MCM-41 catalyst had the worst pyridine oxidation activity because of its highest $T_{100} = 430$ °C value. Also, 2% Cu/MCM-41 showed the poorest ability to control the yield of NO_x, attributable to its narrow temperature window ΔT value of only 20 °C. However, 2% Cu/ZSM-5 did not show the best NO_x control ability, although its oxidation activity was the best. 2% Cu/beta presented the best NO_x control ability, and its ΔT value was as wide as 190 °C, indicating that this catalyst could work very well in a relatively large temperature range.

3.3.4. Characterization of surface copper species

It is evident that the supports have a marked effect on the pyridine oxidation reaction, especially on the NO_x yield. To explain this phenomenon, the nature and chemical state of copper species on different supports are characterized by means of XRD, XPS, and TPR techniques.

3.3.4.1. XRD XRD was carried out to examine the crystalline structure of the catalysts. Fig. 8 clearly shows the XRD patterns of all the copper-loaded catalysts. Neither CuO oxide nor metal Cu diffraction peaks were detected by our method, indicative of high dispersion of all the Cu species on the supports.

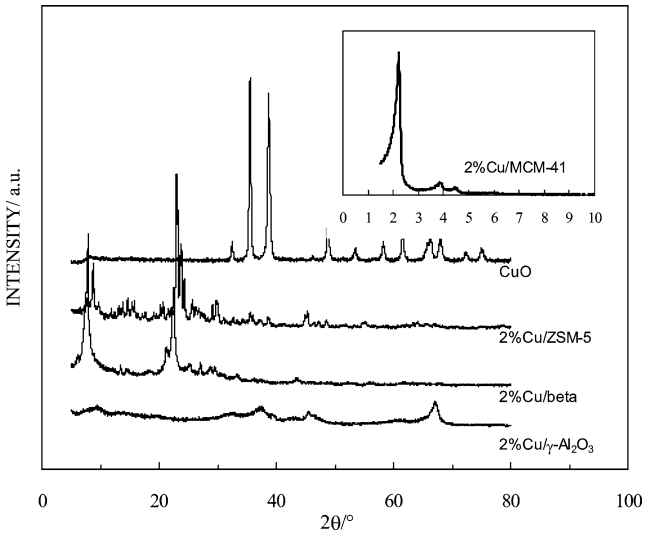

Fig. 8. XRD patterns of supported copper catalysts and pure CuO.

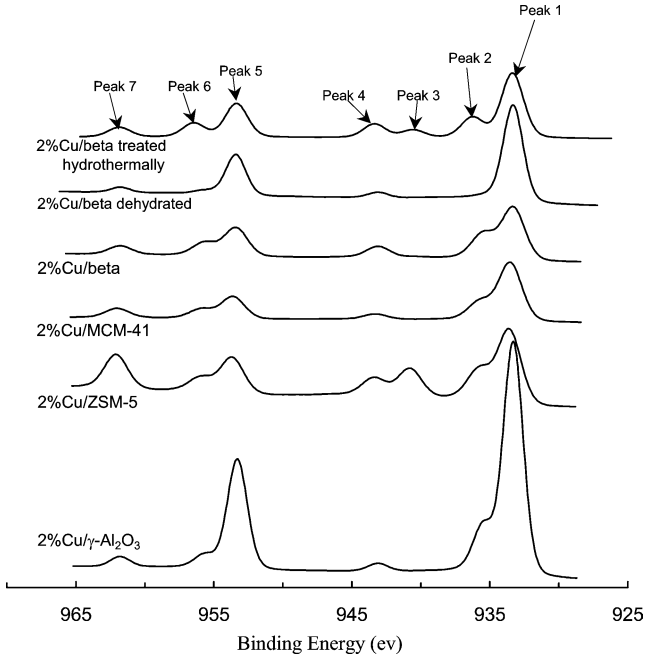

Fig. 9. XPS spectra of Cu 2p of the catalysts 2% Cu/beta (fresh, dehydrated, and treated hydrothermally), 2% Cu/MCM-41, 2% Cu/ZSM-5, and 2% Cu/γ-Al_2O_3.

3.3.4.2. XPS XPS was conducted to provide the information on the elemental compositions and the oxidation state. Fig. 9 illustrates the XPS spectrum of 2% Cu/beta, where peak 1 at 933.29 eV is assigned to $2p_{3/2}$ of Cu^{2+} in the form of CuO according to the literature [37,38]. As we know, the binding energy of Cu^{2+} species ($3d^9$) is about 10 eV higher than that of Cu $2p_{3/2}$ transition; this characteristic is usually used to determine the presence of Cu^{2+} [39]. Fig. 9 clearly shows such a peak 4 at 943.09 eV, which is 9.8 eV higher than peak 1, in agreement with the result reported in the literature [37], showing the existence of CuO species in the 2% Cu/beta sample. Cu^{2+} $2p_{1/2}$ in CuO and its satellite peak were detected to locate at 953.50 eV (peak 5) and 961.90 eV (peak 7), respectively, consistent with those reported in the literature [38], further confirming the existence of CuO species in the 2% Cu/beta sample. Moreover, there were still another two peaks, namely peak 2 at 935.60 eV and peak 6 at 956.00 eV (in Fig. 9). To identify peaks 2 and 6, 2% Cu/beta sample was first dehydrated under vacuum at 300 °C for 12 h to result in a dull gray dehydrated sample, and then the XPS spectrum of the dehydrated sample was measured (in Fig. 9). Very clearly, the peak at 935.60 eV was totally removed, and only a very small peak appeared at 956.00 eV. Narayana et al. [40] have attributed the aforesaid two peaks to $Cu(H_2O)_6^{2+}$ complex locating in the large cages of zeolite, namely the isolated Cu^{2+} ions. Actually, the existence of hydrated Cu^{2+} ions has been indicated by the light green color of as-prepared 2% Cu/beta catalyst.

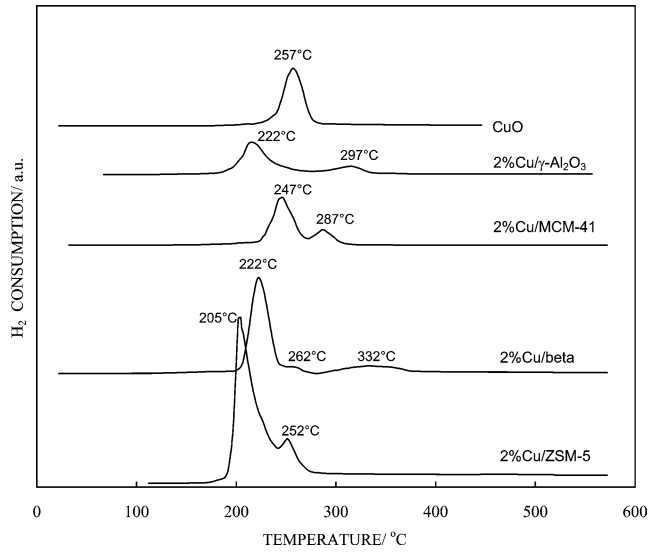

Fig. 10. H_2-TPR profiles of different copper-containing catalysts.

The XPS spectra of Cu species obtained from 2% Cu/ZSM-5 (933.4, 935.6, 940.5, 943.1, 953.5, 956.0, and 961.8 eV), 2% Cu/MCM-41 (933.2, 935.6, 943.0, 953.4, 956.0, and 961.8 eV) and 2% Cu/γ-Al_2O_3 (933.3, 935.6, 943.1, 953.5, 956.0, and 961.9) (in Fig. 9), showing that both CuO and Cu^{2+} ions also coexisted in these catalysts. By comparing the area of XPS peaks of CuO and Cu^{2+} ions, we can come to a conclusion that the copper species in these catalysts are mainly present in the form of CuO, which is further confirmed by TPR tests.

3.3.4.3. TPR TPR profiles of different copper-loaded catalysts, and pure CuO oxide which is used as a reference, are presented in Fig. 10. It was found that for pure CuO oxide only one reduction peak emerged at 257 °C, while for all the supported copper catalysts there were two reduction peaks. 2% Cu/beta displayed two main TPR peaks at 222 and 332 °C, with a shoulder peak at 262 °C. The peak at 222 °C was ascribable to the reduction of CuO to metal Cu^0, the peak at 262 °C to the reduction of Cu^{2+} to Cu^+ ions,

and the peak at 332 °C to the reduction of Cu^+ to metal Cu^0, respectively. It has been reported that the supports could enhance the reduction of copper oxide species [41], and the reduction temperature of CuO in the CuO/SiO_2 decreased from 297 to 227 °C, along with increasing the dispersion of CuO on silica [42,43], in agreement with other results reported elsewhere [44,45]. The ratio of the area of the first peak to the second peak (in Fig. 10) indicated that highly dispersed CuO was a main form of copper species on beta. The reduction peak temperature of the catalysts (in Fig. 10) increased in the order of 2% Cu/ZSM-5 < 2% Cu/beta ≈ 2% Cu/γ-Al_2O_3 < 2% Cu/MCM-41, inversely proportional to the decreasing sequence of their pyridine oxidation activity, namely 2% Cu/MCM-41 < 2% Cu/beta < 2% Cu/γ-Al_2O_3 < 2% Cu/ZSM-5, suggesting that the copper species reduced easily at lower temperatures had higher oxidation activity.

The preceding results have shown that there were two kinds of copper species on supports, namely, CuO and $Cu(H_2O)_6^{2+}$. The percentage of $Cu(H_2O)_6^{2+}$ ions in total copper amount was determined to be around 26.5% for 2% Cu/beta, 21.9% for 2% Cu/MCM-41, 18.1% for 2% Cu/ZSM-5, and 15.3% for 2% Cu/γ-Al_2O_3, respectively. This sequence was almost the same as that of NO_x control ability of these catalysts with an exception of 2% Cu/MCM-41, which showed the poorest NO_x control ability in the pyridine oxidation, further suggesting that $Cu(H_2O)_6^{2+}$ together with some other factors like the nature of the support took critical roles in retarding the NO_x yield of pyridine oxidation. Many researchers have reported that Cu^{2+} ions were much more active than CuO in the SCR deNO_x reaction [46], consistent with our results that $Cu(H_2O)_6^{2+}$ ions really possessed a better NO_x control ability than CuO. This has been further proven in our hydrothermal treatment experiments in which 2% Cu/beta catalyst was hydrothermally treated at 600 °C for 12 h in a helium flow containing 10% water vapor, prior to catalytic tests. It was found that the hydrothermally treated 2% Cu/beta showed a slightly improved oxidation activity but a noticeably worse NO_x control ability in comparison with the untreated one for the pyridine oxidation.

3.3.5. Effect of hydrothermal treatment on the Cu/beta catalyst

As described above, Cu/beta was one of the most promising catalysts for the pyridine oxidation. Recently, some researchers [45,47] reported the low stability of Cu/ZSM-5 catalyst in the presence of water vapor, which is a typical condition of diesel engine exhaust gas. As a result, it is worthwhile to investigate the resistance of Cu/beta catalyst to water vapor. To fulfill this target, 2% Cu/beta catalyst was treated hydrothermally at 600 °C for 12 h in a helium flow containing 10% water vapor, prior to catalytic tests. The hydrothermal treatment slightly improved the oxidation activity of 2% Cu/beta catalyst for the pyridine oxidation, in which the hydrothermally treated 2% Cu/beta showed a stronger pyridine oxidation ability than the untreated one at reaction temperatures between 300 and 350 °C. The temperature (T_{100}) required for the complete oxidation of pyridine was 400 °C for the treated 2% Cu/beta and 410 °C for the untreated 2% Cu/beta, respectively. Additionally, an obvious increase of NO_x yield was observed to be from 20% over the untreated catalyst to 26% over the treated one at 700 °C, and ΔT value dropped from 190 °C of untreated catalyst to 140 °C of treated one.

The hydrothermal treatment has resulted in the appearance of a new XPS peak at the XPS spectrum of treated 2% Cu/beta sample. In Fig. 9, peak 3 at about 940.6 eV can be observed for both 2% Cu/beta treated hydrothermally (933.2, 935.7, 940.6, 943.0, 953.4, 956.0, and 961.8 eV) and 2% Cu/ZSM-5 (933.4, 935.6, 940.5, 943.1, 953.5, 956.0, and 961.8 eV). Thus, it is not likely that peak 3 at about 940.6 eV belongs to ZSM-5. In addition, this peak has also been observed from XPS spectrum (not shown in Fig. 9) of 6% Cu/MCM-41 (933.2, 935.4, 940.6, 942.8, 953.4, 956.0, and 961.9 eV), further indicating that peak 3 at 940.6 eV is not from ZSM-5. However, peak 3 at about 940.6 eV cannot be observed at all for 2% Cu/γ-Al_2O_3, 2% Cu/beta and 2% Cu/MCM-41. Based on these experiments, we can come to a conclusion that peak 3 could result from Cu species, especially from highly crystallized CuO instead of highly dispersed CuO.

By comparing the XPS spectra of untreated 2% Cu/beta and treated one (in Fig. 9), it was found that the hydrothermal treatment led to a reduction of the amount of $Cu(H_2O)_6^{2+}$ in the catalyst, with a percentage drop from 26.5 to 20.7%. As reported by other authors [45,46], the decrease of activity of ion-exchanged Cu/ZSM-5 catalyst in the deNO_x reaction is that most of the isolated Cu^{2+} ions were converted to CuO by the hydrothermal treatment. The aforesaid results have shown that CuO had a better oxidation activity but a poorer ability to reduce the yield of NO_x than Cu^{2+} ions, and that the NO_x control ability varied with different supports. Thus, the loss of $Cu(H_2O)_6^{2+}$ ions converted to CuO oxides on beta during the hydrothermal treatment could be a partial reason for the fact that the 2% Cu/beta catalyst treated hydrothermally suffered from a loss in the NO_x control ability. Generally speaking, a deciding role in the NO_x control ability of the catalysts could involve the cointeraction of some factors, such as the surface acidity of catalysts, the structure of supports, and the amount of $Cu(H_2O)_6^{2+}$ ions on the supports.

4. Conclusions

The activity of supported copper catalysts for the pyridine oxidation increased with the increase of copper content from 0 to 6 wt%. Further increasing the copper content showed no contribution in improving the pyridine oxidation activity of the resulting catalyst. The NO_x control ability (ΔT) of Cu-loaded catalysts went through a maximum value with the

increase of copper content from 0 to 15 wt%. 2% Cu/beta exhibited the best NO_x control ability with a ΔT value of 190 °C, while the ΔT value of 6% Cu/beta dropped to 140 °C. When the catalyst worked in a rather low temperature range, 6% Cu/beta showed a better activity, because it could completely convert pyridine at only 310 °C. However, in a high temperature range from 400 to 700 °C, 2% Cu/beta was supposed to be a better choice, as it showed a better NO_x control ability. Pyridine oxidation ability and NO_x control ability could not be correlated with the surface area of the catalysts at all.

Cu/beta was the most active one among Cu/beta, Fe/beta, Co/beta, and Ni/beta catalysts, and the catalyst that could be reduced at lower temperature had a better oxidation activity. The number of Brønsted acid sites of four acidic supports decreases in the following sequence ZSM-5 (3.80) > beta (1.66) > γ-Al_2O_3 (1.41) > MCM-41 (0.59); while that of their Lewis acid sites decreases in a new order of beta (4.23) > ZSM-5 (1.05) > γ-Al_2O_3 (0.75) > MCM-41 (0.62). It seems that the better NO_x control ability can be attributed to the importance of Lewis acidity of samples, rather than to that of Brønsted acidity.

2% Cu/beta, 2% Cu/ZSM-5 and 2% Cu/γ-Al_2O_3 exhibited a similar pyridine oxidation activity tendency and a close T_{100} value about 390 °C. 2% Cu/MCM-41 was less active for the pyridine oxidation as its T_{100} value was high up to 430 °C. At a reaction temperature as high as 700 °C, the NO_x yield of 2% Cu/beta, 2% Cu/ZSM-5, 2% Cu/MCM-41, and 2% Cu/γ-Al_2O_3 were 20, 30, 37, and 33%, respectively. It was found that $Cu(H_2O)_6^{2+}$ ions showed a better NO_x control ability but poorer activity for the pyridine oxidation than CuO oxides, and that the NO_x control ability varied with different supports. The hydrothermal treatment retarded the NO_x control ability of 2% Cu/beta catalyst, partially due to the loss of $Cu(H_2O)_6^{2+}$ ions converted to CuO oxides on beta during the hydrothermal treatment. The cointeraction of some factors, such as the surface acidity of catalysts, the structure of supports, and the amount of $Cu(H_2O)_6^{2+}$ ions on the supports, played a deciding role in the NO_x control ability of the catalysts.

References

[1] Z.R. Ismagilov, M.A. Kerzhentsev, Catal. Rev.-Sci. Eng. 32 (1990) 51.
[2] Z.R. Ismagilov, M.A. Kerzhentsev, V.I. Besedin, T.L. Susharina, React. Kinet. Catal. Lett. 23 (1983) 43.
[3] Z.R. Ismagilov, M.A. Kerzhentsev, V.I. Besedin, T.L. Susharina, React. Kinet. Catal. Lett. 23 (1983) 49.
[4] M.F. Luo, Y.J. Zhong, M. Chen, B. Zhu, X.X. Yuan, Environ. Sci. 17 (1996) 52.
[5] M.F. Luo, M. Yu, X.X. Yuan, Chinese J. Appl. Chem. 12 (1995) 87–89.
[6] N. Crain, S. Tebbal, L. Li, E.F. Golyna, Ind. Eng. Chem. Res. 32 (1993) 2259.
[7] T.J. Wightman, Studies in Supercritical Wet Air Oxidation, M.S. thesis, University of California at Berkeley, Berkeley, CA, 1981.
[8] A.R. Katritzky, R.A. Barcock, Energy Fuels 8 (1994) 990.
[9] S.N.V.K. Aki, M.A. Abraham, Chem. Eng. Sci. 54 (1999) 3533.
[10] Q.H. Xia, S.C. Shen, J. Song, S. Kawi, K. Hidajat, J. Catal. 219 (2003) 74.
[11] K.J. Chao, T.C. Tasi, M.S. Chen, I. Wang, J. Chem. Soc., Faraday Trans. 1 76 (1981) 77.
[12] R.A. Kensington, G.R. Landolt, US patent 3,702,886, 1972.
[13] S.C. Shen, S. Kawi, Chem. Lett. (1999) 1293.
[14] S.C. Shen, S. Kawi, Stud. Surf. Sci. Catal. 129 (2000) 227.
[15] P.W. Park, J.S. Ledford, Appl. Catal. B 15 (1998) 221.
[16] J. Sárkány, J.L. d'Itri, W.M.H. Sachtler, Catal. Lett. 16 (1992) 241.
[17] P.A. Jacobs, M. Tielen, J. Linart, J.B. Uytterhoeven, H. Beyer, J. Chem. Soc., Faraday Trans. 1 72 (1976) 2793.
[18] S.J. Gentry, N.W. Hurst, A. Jones, J. Chem. Soc., Faraday Trans. 1 75 (1979) 1688.
[19] M.C. Campa, V. Indovina, G. Minelli, G. Moretti, I. Pettiti, P. Porta, A. Riccio, Catal. Lett. 23 (1993) 141.
[20] R.S. Cruz, A.J.S. Mascarenhas, H.M.C. Andrade, Appl. Catal. B 18 (1998) 223.
[21] Y.J. Li, T.L. Slager, J.N. Armor, J. Catal. 150 (1994) 388.
[22] E.E. Unmuth, L.H. Schwartz, J.B. Butt, J. Catal. 63 (1980) 404.
[23] R. Brown, M.E. Cooper, D.A. Whan, Appl. Catal. 3 (1982) 177.
[24] O.J. Wimmers, P. Arnoldy, J.A. Moulijn, J. Phys. Chem. 90 (1986) 1331.
[25] F. Mahoney, R. Rudham, J.V. Summers, J. Chem. Soc., Faraday Trans. 1 75 (1979) 314.
[26] K. Inamura, R. Iwamoto, A. Iino, T. Takyu, J. Catal. 142 (1993) 274.
[27] H.Y. Chen, W.M.H. Sachtler, Catal. Today 42 (1998) 73.
[28] B. Coq, M. Mauvezin, G. Delahay, S. Kieger, J. Catal. 195 (2000) 298.
[29] T.V. Voskoboinikov, H.Y. Chen, W.M.H. Sachtler, Appl. Catal. B 19 (1998) 279.
[30] J.F. Jia, J.Y. Shen, L.W. Lin, Z.S. Xu, T. Zhang, D.B. Liang, J. Mol. Catal. A: Chem. 138 (1999) 177.
[31] M.V. Cagnoli, N.G. Gallegos, A.M. Alvarez, J.F. Bengoa, A.A. Yeramián, M. Schmal, S.G. Marchetti, Appl. Catal. A 230 (2002) 169.
[32] R.Q. Long, R.T. Yang, J. Catal. 194 (2000) 80.
[33] B.W. Hoffer, A.D. Langeveld, J.P. Janssens, R.L.C. Bonné, C.M. Lok, J.A. Moulijn, J. Catal. 192 (2000) 432.
[34] B. Vos, E. Poels, A. Bliek, J. Catal. 198 (2001) 77.
[35] M. Afzal, G. Yasmeen, M. Saleem, J. Afzal, J. Therm. Anal. Calor. 62 (2000) 277.
[36] J.Y. Yan, G.D. Lei, W.M.H. Sachtler, H.H. Kung, J. Catal. 161 (1996) 43.
[37] J.F. Xu, W. Ji, Z.X. Shen, S.H. Tang, X.R. Ye, D.Z. Jia, X.Q. Xin, J. Solid State Chem. 147 (1997) 516.
[38] R.P. Vasquez, Surf. Sci. Spect. 5 (1998) 262.
[39] M.A. Kohler, H.E. Curry-Hyde, A.E. Hughes, B.A. Sexton, N.W. Cant, J. Catal. 108 (1987) 323.
[40] M. Narayana, S. Contatini, L. Kevan, J. Catal. 94 (1985) 370.
[41] Y.H. Hu, L. Dong, M.M. Shen, D. Liu, J. Wang, W.P. Ding, Y. Chen, Appl. Catal. B 31 (2001) 61.
[42] S.D. Robertson, B.D. McNicol, J.H. de Baas, S.C. Cloet, J.W. Jenkins, J. Catal. 37 (1975) 424.
[43] F.S. Delk, A. Vavera, J. Catal. 85 (1984) 380.
[44] G. Delahay, B. Coq, L. Broussous, Appl. Catal. B 12 (1997) 49.
[45] C. Torre-Abreu, M.F. Ribeiro, C. Henriques, G. Delahay, Appl. Catal. B 12 (1997) 249.
[46] K.C.C. Kharas, H.J. Robota, D.J. Liu, Appl. Catal. B 2 (1993) 225.
[47] C.E. Quincoces, A. Kikot, E.I. Basaldella, M.G. Gonzalez, Ind. Eng. Chem. Res. 38 (1999) 4236.